Study of the decays $D \to K 3\pi$

J. C. Anjos,[c] J. A. Appel,[f] A. Bean,[a] S. B. Bracker,[k] T. E. Browder,[a,*] L. M. Cremaldi,[g] J. E. Duboscq,[a] J. R. Elliott,[e,†] C. O. Escobar,[j] M. C. Gibney,[e,‡] G. F. Hartner,[k] J. Huber,[a] P. E. Karchin,[l] B. R. Kumar,[k] M. J. Losty,[h] G. J. Luste,[k] P. M. Mantsch,[f] J. F. Martin,[k] S. McHugh,[a] S. R. Menary,[k,§] R. J. Morrison,[a] T. Nash,[f] J. Pinfold,[b] G. Punkar,[a,**] M. V. Purohit,[i] W. R. Ross,[l] A. F. S. Santoro,[c] D. M. Schmidt,[a] A. L. Shoup,[d,††] K. Sliwa,[f,‡‡] M. D. Sokoloff,[d] M. H. G. Souza,[c] D. Sperka,[a] W. J. Spalding,[f] M. E. Streetman,[f] A. B. Stundžia,[k] and M. S. Witherell[a]

[a]*University of California, Santa Barbara, California, 93106*
[b]*Carleton University, Ottawa, Ontario, Canada K1S5B6*
[c]*Centro Brasileiro de Pesquisas Fisicas, Rio de Janeiro, Brazil*
[d]*University of Cincinnati, Cincinnati, Ohio 45221*
[e]*University of Colorado, Boulder, Colorado 80309*
[f]*Fermi National Accelerator Laboratory, Batavia, Illinois 60510*
[g]*University of Mississippi, Oxford, Mississippi 38677*
[h]*National Research Council, Ottawa, Ontario, Canada K1A0R6*
[i]*Princeton University, Princeton, New Jersey 08544*
[j]*Universidade de São Paulo, São Paulo, Brazil*
[k]*University of Toronto, Toronto, Ontario, Canada M5S1A7*
[l]*Yale University, New Haven, Connecticut 06511*

(Received 2 March 1992)

We report measurements of the decays $D^0 \to K^-\pi^+\pi^+\pi^-$, $D^+ \to \bar{K}^0\pi^+\pi^+\pi^-$, $D^+ \to K^-\pi^+\pi^+\pi^0$, and $D^0 \to \bar{K}^0\pi^+\pi^-\pi^0$ from Fermilab photoproduction experiment E691. A complete resonant substructure analysis is used to determine the relative fractions and phases of amplitudes contributing to the decays $D^0 \to K^-\pi^+\pi^+\pi^-$, $D^+ \to \bar{K}^0\pi^+\pi^+\pi^-$, and $D^+ \to K^-\pi^+\pi^+\pi^0$.

PACS number(s): 13.25.+m, 14.40.Jz

I. INTRODUCTION

Extensive theoretical predictions have been made for D mesons decaying into two-body states [1–4]. These include decays to pseudoscalar-pseudoscalar (PP), pseudoscalar-vector (PV), and vector-vector (VV), and pseudoscalar–axial-vector (PA) states. Of these, the VV and PA decays are not well measured because of the high V and A decay multiplicity and the difficulty of extracting resonant components. Despite these predictions for two-body decays, virtually nothing is predicted about the size of many-body decays, although they may contribute significantly to the total width of channel mesons. In some cases, estimates of lifetimes are made by adding up the two-body decays, ignoring other channels. It is therefore important to measure the size of the PA and VV decays and to determine whether the multibody decays are large.

At present, a large fraction of the hadronic decays of D^0 and D^+ mesons has been accounted for experimentally. Measurements exist for the Cabibbo-allowed decays into $K\pi$, $K\pi\pi$, $K4\pi$, as well as $K3\pi$ [5–7]. The photoproduction data taken by Fermilab experiment E691 provides an excellent opportunity to measure the vector-vector and pseudoscalar–axial-vector modes of charm decay. In this experiment, large background suppression is achieved for high multiplicity modes by observing the separated charm vertex. In this paper, measurements of the $D^0 \to K^-\pi^+\pi^+\pi^-$, $D^0 \to \bar{K}^0\pi^+\pi^-\pi^0$, $D^+ \to \bar{K}^0\pi^+\pi^+\pi^-$, and $D^+ \to K^-\pi^+\pi^+\pi^0$ decays are presented.

II. EVENT SELECTION

The D^0 and D^+ samples used in this study were obtained from the analysis of the full data sample of 10^8 events from Fermilab photoproduction experiment E691. This experiment collected data using the Tagged Photon Spectrometer [8], which is a large acceptance two-magnet spectrometer with silicon microstrip detectors, drift chambers, Cherenkov counters, and both electromagnetic and hadronic calorimetry. A bremsstrahlung photon beam with energy in the range 90–260 GeV was directed to a 5-cm beryllium target. Events with a transverse energy greater than 2.2 GeV were recorded. A general vertex reconstruction was first performed and events with

*Now at Cornell University, Ithaca, NY 14853.
†Now at Electromagnetic Applications, Inc., Denver, CO 80226.
‡Now at Nichols Research Inc., Colorado Springs, CO 80919.
§Now at University of California, Santa Barbara, CA 93106-9530.
**Now at SLAC, P.O. Box 4349, Stanford, CA 94309.
††Now at University of California, Irvine, CA 92716.
‡‡Now at Tufts University, Medford, MA 02155.

fitted vertices having $\chi^2/N_{DF}<3$ were retained. Next it was required that all charged tracks except those from the decay of K_S^0 traversed both spectrometer magnets and had momenta of at least 3 GeV/c. This minimum momentum cutoff is applied to ensure that there are enough drift chamber hits to form a track that can be well modeled in our Monte Carlo simulation. The reconstructed momenta of the decay (charm) vertex products was required to point back to the production vertex within 80 μm for the $K^-\pi^+\pi^+\pi^-$ and $\bar{K}^0\pi^+\pi^+\pi^-$ channels and within 100 μm for the channels containing a π^0. Only events with four-body mass in the range 1.75–2.00 GeV/c^2 were used in the subsequent analysis.

Neutral pions were found using two well-identified photons with a mass consistent with the π^0. To suppress background, only π^0s with energy greater than 8 GeV were used. Figure 1 shows the $\gamma\gamma$ mass spectra in the π^0 mass region. Typical π^0 identification efficiencies are around 18% for multibody hadronic charm meson decays. The acceptance only depends slightly on the kinematic variables in the D meson rest frame, and this effect can be modeled reliably because of the sharp cutoff on the π^0 energy in the laboratory. We observed $\bar{K}^0$ decays through the decay $K_S^0\to\pi^+\pi^-$ which occurred downstream of the silicon microstrip detector. K_S^0 candidates were found by forming two-track vertices using tracks detected in the 35 plane drift chamber system. The distance of closest approach of the two tracks was required to be less than 0.5 cm and the $\pi^+\pi^-$ invariant mass had to be between 0.480 and 0.514 GeV/c^2. Decay pions from this vertex were required to have a combined Cherenkov probability of greater than 0.1. This cut means that all the tracks are consistent with being pions.

Events for the $D^0\to K^-\pi^+\pi^+\pi^-$ analysis were selected with the additional requirement that the combination of four tracks had a joint Cherenkov probability of 0.15 or greater. This is a requirement that the kaon be positively identified in the Cherenkov counter and other tracks are consistent with pion identification. For events consistent with the decay $D^{*+}\to D^0\pi^+$, $D^0\to K^-\pi^+\pi^+\pi^-$, we required $6<S_z=\Delta z/\sigma_z\le 15$ where Δz is the separation between the production vertex and the charm vertex in the beam z direction and σ_z is the measurement error of the vertex separation [8]. These events also were required to have a fifth track with momentum greater than 1 GeV/c, a pion Cherenkov identification probability greater than 0.2, and momentum consistent with a D^{*+} decay. We also included events with $S_z>15$ and no D^{*+} cuts. The D^{*+} requirement greatly improves the signal to background but also has no effect on the resonance subcomponent contribution since it is independent of the D^0 decay . The data sample yielded a signal of 1745 events over a background of 800. Figure 2 shows the invariant $K^-\pi^+\pi^+\pi^-$ mass plot. The fit, which is described in more detail later, is represented in the figures by filling mass bins with signal (background) contributions from the reconstructed Monte Carlo (phase space) data weighted by the appropriate terms from the likelihood function. We measure the ratio by branching fractions to be

$$R=\frac{B(D^0\to K^-\pi^+\pi^+\pi^-)}{B(D^0\to K^-\pi^+)}=1.7\pm0.2\pm0.2\ .$$

If we use Mark III's measurement [6] of $B(D^0\to K^-\pi^+)=(4/2\pm0.4\pm0.4)\%$ we find $B(D^0\to K^-\pi^+\pi^+\pi^-)=(7.1\pm1.1\pm1.1)\%$, which agrees with the Mark III measurement of $B(D^0\to K^-\pi^+\pi^+\pi^-)=(9.1\pm0.8\pm0.8)\%$ [6].

For the channel $D^0\to\bar{K}^0\pi^+\pi^-\pi^0$, two independent samples were obtained with identified π^0's: those consistent with the decay of $D^{*+}\to D^0\pi^+$ and those not from a D^{*+} decay. For the sample obtained from the D^{*+}, a cut was made on the mass difference between the D^{*+} and D^0 requiring a slow pion, with $S_z>8$. The second sample included events with $S_z\ge 15$ and excluded events consistent with D^{*+} decay.

Figure 3(a) shows the $\bar{K}^0\pi^+\pi^-\pi^0$ invariant mass plot for events consistent with a D^0 coming from a D^{*+}. The fit finds 16.3±5.6 events. The significance of this signal compared to the hypothesis of zero events is 3.6σ. Figure 3(b) shows the invariant mass plot for those events

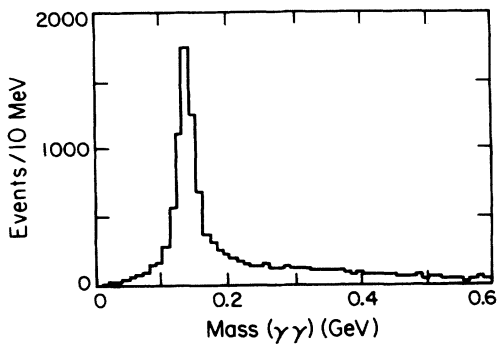

FIG. 1. $\gamma\gamma$ invariant mass for a typical π^0 signal after applying the π^0 cuts.

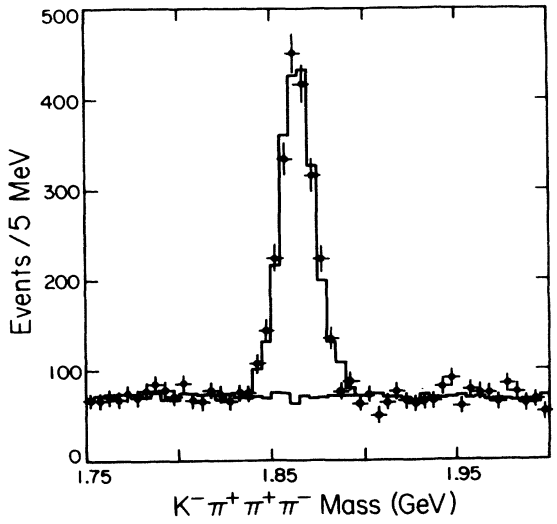

FIG. 2. $K^-\pi^+\pi^+\pi^-$ invariant mass. Data are shown using the points with error bars, the top histogram indicates the fit, while the lower histogram shows the fitted background.

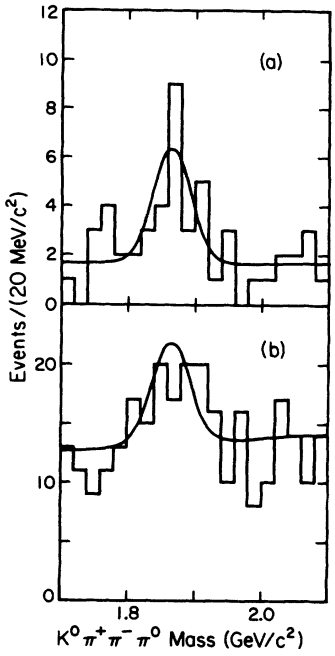

FIG. 3. $\bar{K}^0\pi^+\pi^-\pi^0$ invariant mass for (a) events consistent with the decay $D^{*+} \to D^0\pi^+$, (b) events with the D^{*+} decay hypothesis excluded.

not having a D^{*+}. There are 29.5 ± 11.9 events in the peak, also a 3.6σ effect. The ratio of branching fractions in the first sample is

$$R = \frac{B(D^0 \to \bar{K}^0\pi^+\pi^-\pi^0)}{B(D^0 \to \bar{K}^0\pi^+\pi^-)} = 3.0\pm1.1\pm0.8 ,$$

while the second sample gives $R = 2.6\pm1.2\pm0.8$. The combined ratio of both samples gives $R = 2.8\pm0.8\pm0.8$. Using the branching fraction measured by Mark III [6] for $D^0 \to \bar{K}^0\pi^+\pi^-$ of $(5.6^{+0.7}_{-0.6})\%$, we find

$$B(D^0 \to \bar{K}^0\pi^+\pi^-\pi^0) = (15.7\pm4.9\pm4.5)\% .$$

There were not enough events in this mode to perform a resonant subcomponent analysis.

For the D^+ candidates we required $S_z > 15$ and no extra tracks passing within 80 μm of the decay vertex. All tracks in the decay vertex were required to pass closer to the decay vertex than to the production vertex, which reduces the efficiency by only a few percent and has no differential effect on the angular distribution. (The small acceptance hole in the laboratory frame is randomly oriented with respect to any performed direction in the D rest frame because the D is a spinless particle.) For the $D^+ \to \bar{K}^0\pi^+\pi^+\pi^-$ analysis the decay vertex included

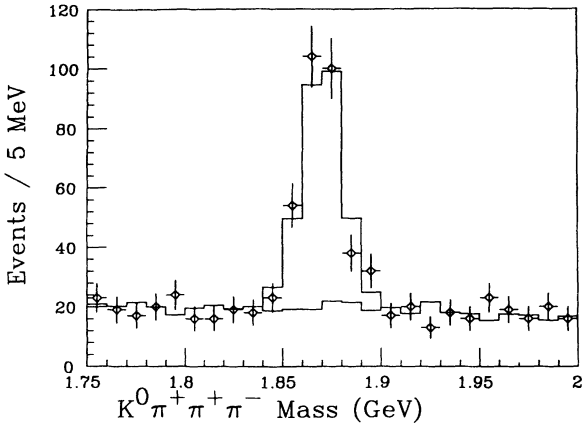

FIG. 4. $\bar{K}^0\pi^+\pi^+\pi^-$ invariant mass. Data are shown as in Fig. 2.

only the 3 pions. The three charged tracks in the decay vertex were required to have a combined Cherenkov probability of greater than 0.12. The sample consisted of 229.4 ± 17.0 events over a background of 133 events. This is shown in Fig. 4. After correcting for the $\bar{K}^0 \to K^0_S$ and $K^0_S \to \pi^+\pi^-$ branching fractions, the relative branching fraction of

$$R = \frac{B(D^+ \to \bar{K}^0\pi^+\pi^+\pi^-)}{B(D^+ \to K^-\pi^+\pi^+)} = 0.77\pm0.07\pm0.11$$

is found. Combined with the Mark III [6] branching fraction for $D^+ \to K^-\pi^+\pi^+$ of $(9.1\pm1.3\pm0.4)\%$ one finds the value for $B(D^+ \to \bar{K}^0\pi^+\pi^+\pi^-) = (7.0\pm1.2\pm1.0)\%$, which is also given in Table I. This agrees well with the Mark III measurement of $(6.6\pm1.5\pm0.5)\%$ from their sample of 209 ± 20 events [6].

Figure 5 shows the invariant $K^-\pi^+\pi^+\pi^0$ mass spectrum. Events consistent with the decay chain $D^{*+} \to D^0\pi^+$, $D^0 \to K^-\pi^+\pi^0$ were excluded in this analysis. The fit found 90.8 ± 12.4 events at the D^+ mass and 53 events in the background region, which corresponds to a relative branching fraction

$$R = \frac{B(D^+ \to K^-\pi^+\pi^+\pi^0)}{B(D^+ \to K^-\pi^+\pi^+)} = 0.76\pm0.11\pm0.12 .$$

The systematic error comes principally from the uncertainty in modeling the π^0 in the Monte Carlo simulation. Using the Mark III absolute branching fraction for $B(D^+ \to K^-\pi^+\pi^+)$ given earlier [6], we find $B(D^+ \to K^-\pi^+\pi^+\pi^0) = (6.9\pm1.4\pm1.1)\%$ (see Table I).

TABLE I. Relative and absolute branching fractions. The final column uses information on absolute branching fractions from Ref. [6].

Mode A	Mode B	B(mode A)/B(mode B)	B(mode A) (%)
$D^0 \to \bar{K}^0\pi^+\pi^-\pi^0$	$\bar{K}^0\pi^+\pi^-$	$2.8\pm0.8\pm0.8$	$15.7\pm4.9\pm4.5$
$D^+ \to \bar{K}^0\pi^+\pi^+\pi^-$	$K^-\pi^+\pi^+$	$0.77\pm0.07\pm0.11$	$7.0\pm1.2\pm1.1$
$D^+ \to K^-\pi^+\pi^-\pi^0$	$K^-\pi^+\pi^+$	$0.76\pm0.11\pm0.12$	$6.9\pm1.4\pm1.1$

TABLE II. Results for best fit of $D^0 \to K^-\pi^+\pi^+\pi^-$ decay. We normalize all branching fractions directly to the Mark III absolute branching fraction [6] $B(D^0 \to K^-\pi^+\pi^+\pi^-) = (9.1 \pm 0.8 \pm 0.8)\%$. This is because our branching fraction for this mode must be tied to the Mark III absolute branching fraction for $D^0 \to K^-\pi^+$. The definition of the phase is included in the text. The final column includes corrections for the branching ratios of the intermediate resonances such as K^*, a_1, and ρ.

Amplitude	Fraction (%)	Phase	Branching fraction (%)
Four-body nonresonant	$23 \pm 2 \pm 3$	0.0	$2.1 \pm 0.3 \pm 0.3$
$\bar{K}^{*0}(\pi^+\pi^-)_S$	$11 \pm 2 \pm 3$	-2.0 ± 0.1	$1.5 \pm 0.3 \pm 0.4$
$(K^-\rho^0)_v\pi^+$	$5 \pm 3 \pm 2$	-0.7 ± 0.3	$0.5 \pm 0.3 \pm 0.2$
$K^- a_1^+(1260)$	$47 \pm 5 \pm 10$	-2.7 ± 0.1	$8.6 \pm 1.2 \pm 1.9$
$\bar{K}^{*-}\rho^0_{L=0}$	$25 \pm 3 \pm 4$	2.9 ± 0.1	$3.4 \pm 0.5 \pm 0.6$
$\bar{K}^{*0}\rho^0_{L=2}$	$17 \pm 3 \pm 4$	-0.1 ± 0.1	$2.3 \pm 0.5 \pm 0.6$
$K^-\rho^0\pi^+_{\text{tot}}$	$80 \pm 3 \pm 5$		$7.3 \pm 0.7 \pm 0.8$
$\bar{K}^{*0}\pi^+\pi^-_{\text{tot}}$	$20 \pm 4 \pm 2$		$2.7 \pm 0.6 \pm 0.3$
$\bar{K}^{*0}\rho^0_{\text{tot}}$	$13 \pm 2 \pm 2$		$1.8 \pm 0.3 \pm 0.3$

III. FITTING PROCEDURE FOR RESONANT SUBSTRUCTURE

A multidimensional maximum likelihood fit was performed to determine the resonant subcomponent contributions. The fitting procedure used is the same as that done by Mark III [7] for their $K3\pi$ analysis. The input data to the fit are the five two-body masses from each data event. The maximum likelihood fit to the N_{data} real data points minimized the function

$$\sum_{i=1,N_{\text{data}}} -2\ln F(M_i, \mathbf{m}_{2i}; S, M_D, \sigma, \alpha_k, \beta_k) ,$$

where F was the trial probability density function. Here M and $\mathbf{m}_2$ refer to the experimentally measured value of the four-body mass and the set of five independent two-body masses. The parameters S, M_D, and σ represented the measured D signal, mass, and resolution, respectively. The parameters S and M_D were fixed by a preliminary mass fit while the width was determined from the Monte Carlo data. The form of the probability density function F was chosen to be a sum of a background term and a signal term:

$$F = \frac{N_{\text{data}} - S}{N_{\text{data}}} \frac{F_B}{N_B} + \frac{S}{N_{\text{data}}} \frac{F_S}{N_S} ,$$

where $F_B = \epsilon\phi B(M, \mathbf{m}_2, \beta_k)$ and $F_S = \epsilon\phi |A(\mathbf{m}_2, \alpha_k)|^2 \times \exp[-(M - M_D)^2/2\sigma^2]$. The quantities α_k and β_k were used to parametrize the signal and background probability density functions. To maximize the likelihood, the efficiency function ϵ and the four-body phase-space density ϕ, which did not depend on the fit parameters, were factored out of both the signal and background terms, but were accounted for in the Monte Carlo calculation of the normalization constant N_S and N_B.

The background term B was written as an incoherent sum of normalized functions in the form of a nonresonant background plus terms for possible K^* and ρ contributions. The parameters β_k, which included the relative contribution of resonant components to the background and adjustments to the nonresonant background shape, were fixed by fitting to F_B only in the region of data at least $\pm 3\sigma$ away from M_D. The amplitude $A(\mathbf{m}_2, \alpha_k)$ was

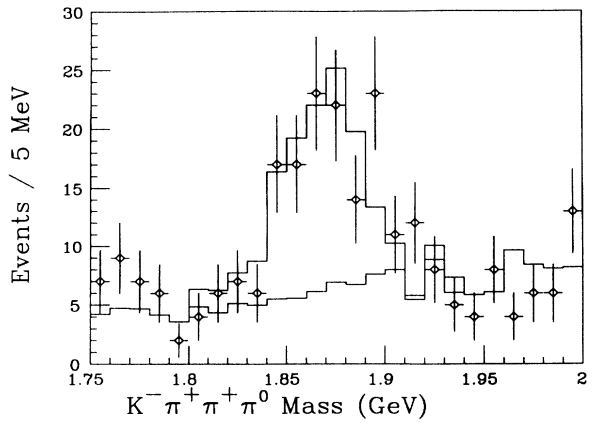

FIG. 5. $K^-\pi^+\pi^+\pi^0$ invariant mass. Data are shown as in Fig. 2.

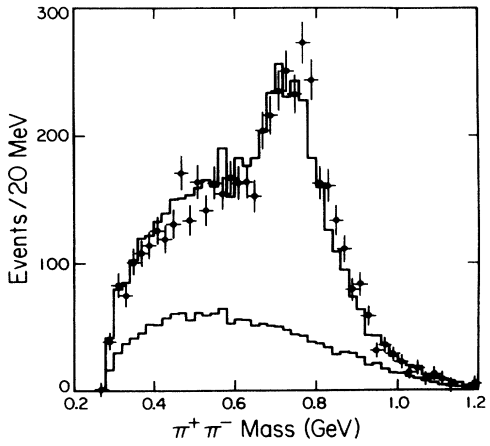

FIG. 6. $\pi^+\pi^-$ invariant mass for events with the $K^-\pi^+\pi^+\pi^-$ mass in the D^0 region. There are two combinations plotted per event. The data are depicted as in Fig. 2.

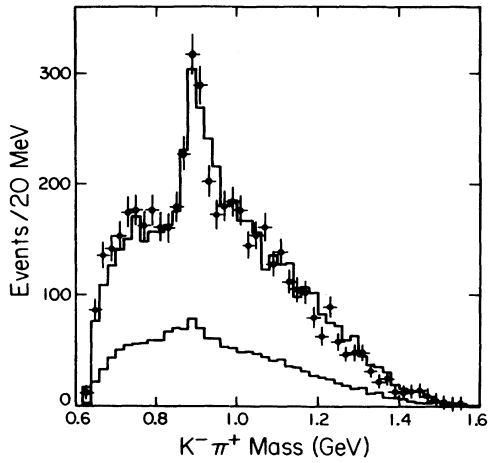

FIG. 7. $K^-\pi^+$ invariant mass for events with the $K^-\pi^+\pi^+\pi^-$ mass in the D^0 regionn. There are two combinations plotted per event. The data are depicted as in Fig. 2.

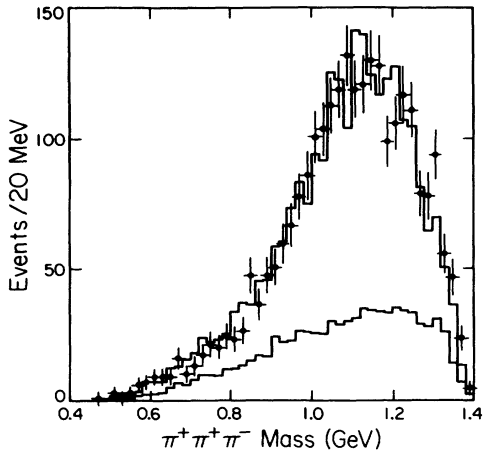

FIG. 8. $\pi^+\pi^+\pi^-$ invariant mass for events with the $K^-\pi^+\pi^+\pi^-$ mass in the D^0 region and is depicted as in Fig. 2.

the sum of complex coefficients α_k times individual Lorentz-invariant matrix elements which were constructed from the measured four momenta of the particles. Relativistic Breit-Wigner forms, with widths corrected for the p^3 dependence of the center-of-mass momentum and modified with a range parameter, were used in the matrix elements [7]. All matrix elements were constructed to be symmetric under the interchange of the identical π^+ in the final decay products.

For the final fit, the Cartesian coordinates of the complex coefficients were the only parameters allowed to vary. Normalization of the likelihood function was done at three levels. First, each individual amplitude was normalized so that the phase-space integral of its square was unity. Second, one amplitude coefficient was fixed and the overall normalization between the signal and background terms was determined by integrating each term over phase space. This integration was done using Monte Carlo methods to account for the efficiency. Finally, the total set of amplitude coefficients was renormalized so that the total phase-space integrated squared amplitude was unity. Relative branching fractions were defined as the square of the individual complex coefficients of the matrix elements and corrected for the appropriate branching fractions of the resonance decay channels. Errors for these and the phases were derived through the covariance matrix as determined by the minimization program.

TABLE III. Limits at 90% confidence level from $D^0 \to K^-\pi^+\pi^+\pi^-$.

Amplitude	Branching fraction (%)
$\bar{K}^{*0}\rho^0_{L=1}$	≤ 0.9
$K_1^-(1270)\pi^+$	≤ 1.3
$K^- a_2^+(1320)$	≤ 0.2
$\bar{K}^{*0} f_0(975)$	≤ 0.7
$K^- f_0(975)\pi^+$	≤ 1.1

IV. $D^0 \to K^-\pi^+\pi^+\pi^-$

For the $D^0 \to K^-\pi^+\pi^+\pi^-$ analysis, amplitudes were defined from Lorentz invariant combinations of the four-momenta and polarization vectors of the decay products. A constant amplitude was defined to model the totally nonresonant contribution to the decay. Next, three-body amplitudes containing either a ρ^0 or $\bar{K}^{*0}$ were defined. For each of these, there were several combinations which differed only by the partial wave of the two nonresonant particles of the decay. Three two-body amplitudes for $\bar{K}^{*0}\rho^0$ were defined corresponding to partial wave content of $L=0$, 1, and 2. Finally, two-body amplitudes containing a higher mass resonance such as $K_1^-(1270)$, $a_1^+(1260)$, and $a_2^+(1320)$ were defined.

There were many possibilities of combinations of these amplitudes for inclusion in the trial fits. This was complicated because different amplitudes were highly correlated, and interfered. A basic fit was defined using only one term for every major resonant mode ($K^*\rho, K\rho\pi, \ldots$). Specifically, only one amplitude for each of the three-body $\bar{K}^{*0}\pi^+\pi^-$ and $K^-\rho^0\pi^+$ channels was included. Additional amplitudes of these types are strongly correlated with each other. It was found that the $\bar{K}^{*0}$ with the $\pi^+\pi^-$ in an s wave [$\bar{K}^{*0}(\pi^+\pi^-)s$] and the ρ^0 with $K^-\rho^0$ in a vector state [$(K^-\rho^0)_v\pi^+$] gave the most significant contribution to these channels. The K^* channel was clearly important, but the significance of the $K\rho\pi$ channel was small and varied with the exact conditions of the fit. Additionally it was found that both an $L=0$ and $L=2\bar{K}^{*0}\rho^0$ amplitude were significant and increased the likelihood. To determine the "best" fit, additional amplitudes with differing partial waves were added in and kept only if they improved the likelihood a significant amount, corresponding roughly to 2σ. The systematic error assigned takes into account the variation in the amplitudes when marginal terms are added to or removed from the fit.

In the best fit we found the largest single component to

TABLE IV. Results for best fit of $D^+ \to \bar{K}^0\pi^+\pi^+\pi^-$ deccay. All branching fractions are calculated assuming $B(D^+ \to \bar{K}^0\pi^+\pi^+\pi^-)=(7.0\pm1.2\pm1.0)$. The definition of the phase in the third column is found in the text. The final column includes corrections for the branching ratios of the intermediate resonances such as K^*, a_1, and ρ.

Amplitude	Fraction (%)	Phase	Branching fraction (%)
Four-body nonresonant	$10\pm4\pm6$	0.0 ± 0.3	$0.7\pm0.3\pm0.4$
$\bar{K}^0\rho^0\pi^+$	$7\pm4\pm6<17$	-2.8 ± 0.2	<1.3
$K^{*-}\pi^+\pi^+_{\text{flat}}$	$33\pm6\pm14$	2.7 ± 0.3	$3.4\pm0.7\pm1.5$
$\bar{K}^0 a_1^+(1260)$	$83\pm14\pm20$	0.0	$11.6\pm2.9\pm3.2$
$\bar{K}^0\rho_0\pi^+_{\text{tot}}$	$60\pm10\pm17$		$4.2\pm1.0\pm1.3$

be due to the $K^- a_1^+(1260)$, $(47\pm5\pm10)\%$ of the total as given in Table II. The only other two-body mode $\bar{K}^{*0}\rho^0$ constitutes only $(13\pm2\pm2)\%$ of the total. Systematic errors were estimated by varying conditions of the fit. These included the width, central mass, and range parameter of the relativistic Breit-Wigner resonance functions. Also taken into account were the Monte Carlo statistics, amount of resonance contribution depending on the choice of the partial wave for the $K^-\rho^0\pi^+$ and $\bar{K}^{*0}\pi^+\pi^-$ terms, and whether or not additional amplitudes for higher mass resonances were included in the fit. The total systematic error was defined by adding the individual systematic errors in quadrature. The errors on the $K^-\rho^0\pi^+$ and $\bar{K}^{*0}\pi^+\pi^-$ terms include the effects of using different partial waves for the two nonresonant particles and the results should be interpreted as the amounts of partial nonresonant contributions irrespective of the specific partial wave. The total of $K^-\rho^0\pi^+$, $\bar{K}^{*0}\pi^+\pi^-$, and $\bar{K}^{*0}\rho^0$ are also shown taking into account the interferences between the various channels. Figures 6 and 7 show the $\pi^+\pi^-$ and $K^-\pi^+$ projections from the best fit. Figures 8 and 9 show the three-body mass combinations for the best fit. Upper limits for additional amplitudes are shown in Table III.

V. $D^+ \to \bar{K}^0\pi^+\pi^+\pi^-$

For the D^+ channels we again had to choose which resonances to include in the fit. Because of the smaller size of the data sample in these channels, a slightly different approach was taken. An initial fit, which was the best for the minimum number of matrix elements, was found to be adequate. An additional component was allowed to remain in the fit only if it increased the log of the likelihood by 4.5, which is equivalent to requiring a 3σ gain by adding the term. After the best fit was found, other terms were added one at a time to determine upper limits on them.

There is no $K^*\rho$ component possible in this channel.

TABLE V. Limits at 90% confidence level from $D^+ \to \bar{K}^0\pi^+\pi^+\pi^-$.

Amplitude	Branching fraction (%)
$\bar{K}_1^0(1270)\pi^+$	≤ 0.7
$\bar{K}_1^0(1400)\pi^+$	≤ 0.9
$\bar{K}^0 a_2^+(1320)$	≤ 0.3
$\bar{K}^0 f_0(975)\pi^+$	≤ 0.5

We looked at the decay channels to (1) nonresonant four-body; (2) three-body $\bar{K}^0\rho^0\pi^+$; (3) three-body $K^{*-}\pi^+\pi^+$; (4) $\bar{K}^0 a_1^+(1260)$, $a_1^+ \to \rho^0\pi^+$; (5) $\bar{K}^0 a_2^+(1320)$, $a_2^+ \to \rho^0\pi^+$; (6) $\bar{K}_1^0(1270)\pi^+$, $K_1 \to \bar{K}^0\rho^0$; (7) $\bar{K}_1^0(1400)\pi^+$, $K_1 \to K^{*-}\pi^+$; and (8) $\bar{K}^0 f_0(975)\pi^+$, $f_0 \to \pi^+\pi^-$. For the three-body amplitudes all two-body combinations in a relative s wave and p wave were tried as well as just the phase-space distribution.

For the initial fit of the background function using the D^+ sidebands, fractions of 33% ρ^0 and 6% K^{*-} were found. The best fit included four terms: nonresonant four-body $\rho^0(\bar{K}^0\pi^+)_s$, phase-space $K^{*-}\pi^+\pi^+$, and $\bar{K}^0 a_1^+(1260)$. Table IV shows the subcomponent fraction, branching fraction, and phase of the coefficient of each component. After determining that most of the branching fraction comes from $\bar{K}^0 a_1^+(1260)$, $(83\pm14\pm20)\%$, we set its phase to zero and measured the remaining phases, including that of the nonresonant component, with respect to it. Table V shows the upper limits of the other terms when added into the best fit one at a time.

The three-body $K\rho\pi$ term marginally improves the fit, but with the systematic error is consistent with zero. The $\rho^0(\bar{K}^0\pi^+)_s$ term gives the best fit and other angular distributions of $K\rho\pi$ not only give poorer fits, but the fraction found is less. Since the $K\rho\pi$ terms are linear combinations of each other, we choose to quote the upper limit for all $K\rho\pi$ as the upper limit obtained using the $\rho(\bar{K}^0\pi^+)_s$ term in the fit. The fit also obviously prefers having the $\bar{K}^0 a_1^+(1260)$ term. The total amount of $K\rho\pi$ in both two-body and three-body modes is the constant given in Table IV. We have accounted for the fluctuation of $\bar{K}^0 a_1^+(1260)$ due to inclusion of three-body $K\rho\pi$

TABLE VI. Results for best fit of $D^+ \to K^-\pi^+\pi^+\pi^0$ decay. All branching fractions are calculated assuming $B(D^+ \to K^-\pi^+\pi^+\pi^0)=(6.9\pm1.4\pm1.1)\%$.

Amplitude	Fraction (%)	Phase	Branching fraction (%)
$K^-\rho^+\pi^+$	$18\pm8\pm4$	2.4 ± 0.4	$1.2\pm0.5\pm0.3$
$\bar{K}^{*0}\pi^+\pi^0$	$44\pm6\pm11$	0.0	$4.5\pm1.2\pm1.3$
$K^{*-}\pi^+\pi^+$	$8\pm4\pm3$	-3.0 ± 0.4	$1.7\pm1.1\pm0.7$
$\bar{K}^{*0}\rho^+_{L=0}$	$10\pm5\pm3$	-2.4 ± 0.2	$1.0\pm0.5\pm0.3$
$\bar{K}^{*0}\rho^+_{L=0}$	$10\pm6\pm3$	1.6 ± 0.3	$1.0\pm0.6\pm0.3$
$K^-\rho^+\pi^+_{\text{tot}}$	$48\pm9\pm3$		$3.3\pm0.9\pm0.6$
$\bar{K}^{*0}\pi^+\pi^0_{\text{tot}}$	$70\pm7\pm5$		$7.2\pm1.6\pm1.3$
$\bar{K}^{*0}\rho^+_{\text{tot}}$	$22\pm11\pm8$		$2.3\pm1.2\pm0.9$

TABLE VII. Limits at 90% confidence level from $D^+ \to K^-\pi^+\pi^+\pi^0$.

Amplitude	Branching fraction (%)
Four-body nonresonant	≤ 0.2
$\bar{K}_1^0(1270)\pi^+$	≤ 19.1
$\bar{K}_1^0(1400)\pi^+$	≤ 0.9
$\bar{K}^{*0}\rho_{L=1}^+$	≤ 0.1

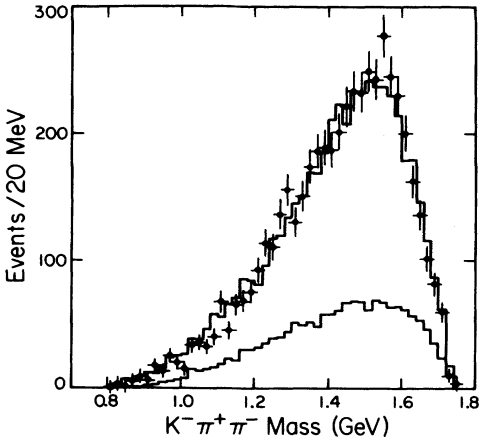

FIG. 9. $K^-\pi^+\pi^-$ invariant mass for events with the $K^-\pi^+\pi^+\pi^-$ mass in the D^0 region. This is depicted as in Fig. 2.

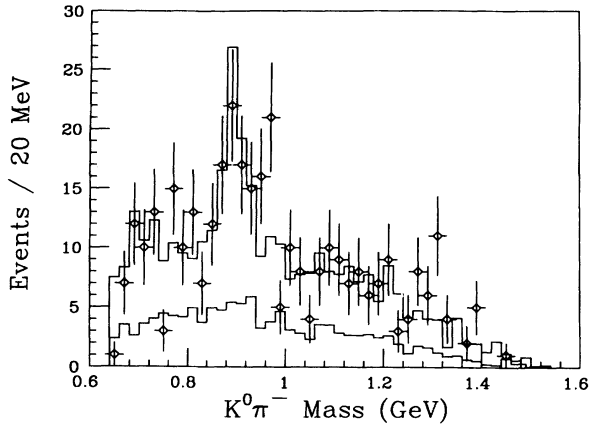

FIG. 11. $\bar{K}^0\pi^-$ invariant mass for events with the $\bar{K}^0\pi^+\pi^+\pi^-$ mass in the D^+ region. The data are depicted as in Fig. 2.

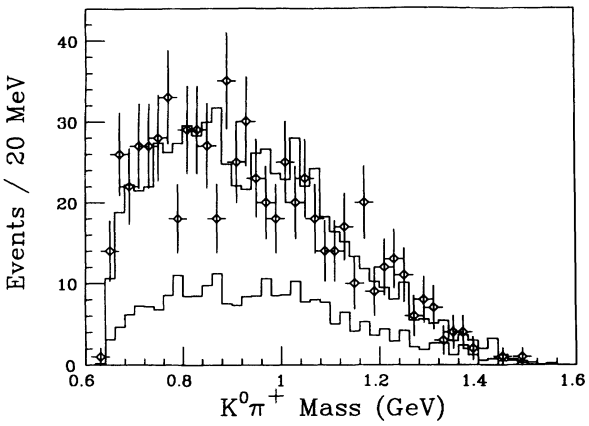

FIG. 12. $\bar{K}^0\pi^+$ invariant mass for events with the $\bar{K}^0\pi^+\pi^+\pi^-$ mass in the D^+ region. There are two combinations plotted per event. The data are depicted as in Fig. 2.

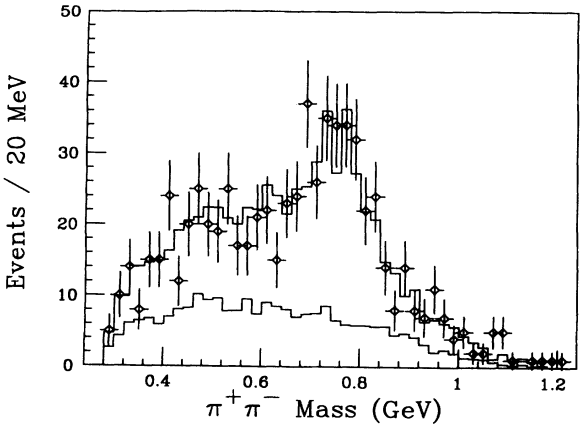

FIG. 10. $\pi^+\pi^-$ invariant mass for events with the $\bar{K}^0\pi^+\pi^+\pi^-$ mass in the D^+ region. There are two combinations plotted per event. The data are depicted as in Fig. 2.

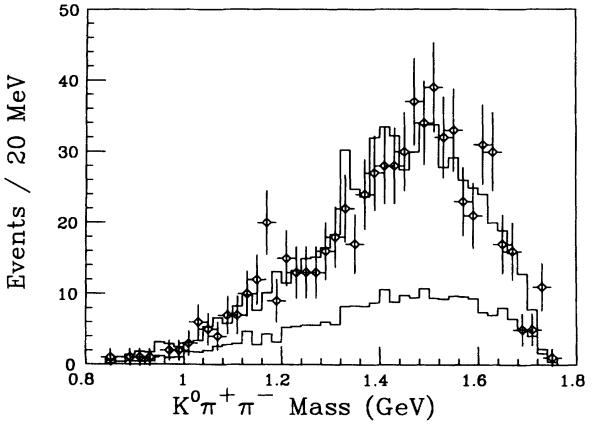

FIG. 13. $\bar{K}^0\pi^+\pi^-$ innvariant mass for events with the $\bar{K}^0\pi^-$ mass in the K^{*-} region. The data are from $\bar{K}^0\pi^+\pi^+\pi^-$ events in the D^+ region and are depicted as in Fig. 2.

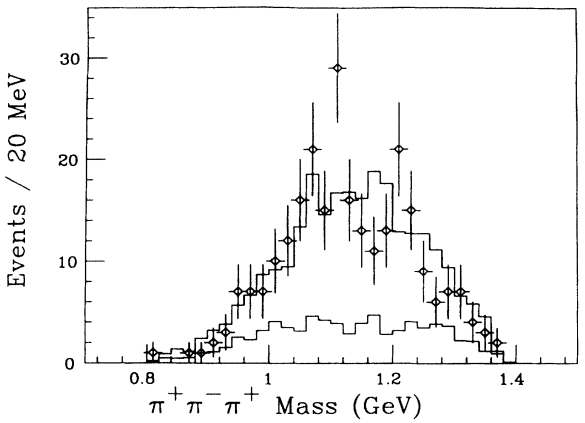

FIG. 14. $\pi^+\pi^-\pi^+$ invariant mass for events with the highest mass $\pi^+\pi^-$ combination in the ρ region. The data are from $\bar{K}^0\pi^+\pi^+\pi^-$ events in the D^+ region and are depicted as in Fig. 2.

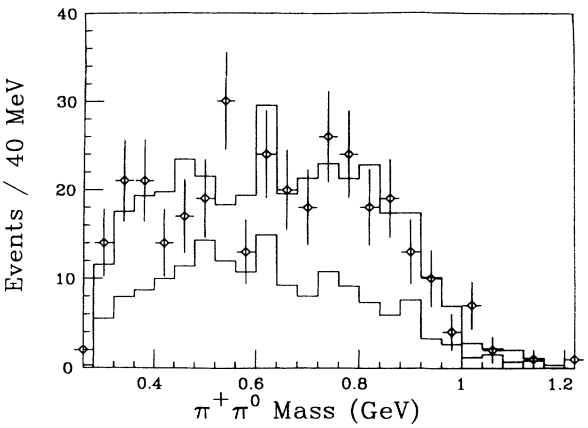

FIG. 17. $\pi^+\pi^0$ invariant mass for events with the $K^-\pi^+\pi^+\pi^0$ mass in the D^+ region. There are two combinations plotted per event. The data are depicted as in Fig. 2.

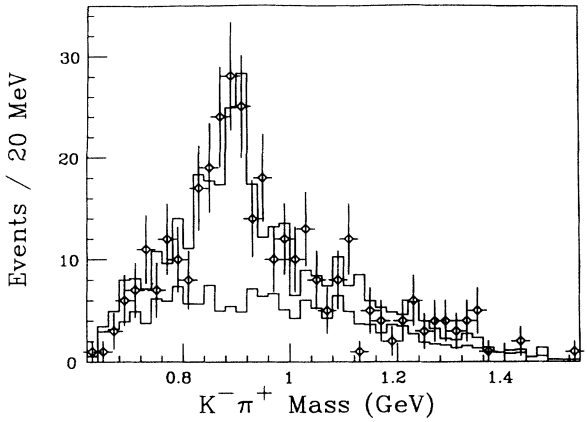

FIG. 15. $K^-\pi^+$ invariant mass for events with the $K^-\pi^+\pi^+\pi^0$ mass in the D^+ region. There are two combinations plotted per event. The data are depicted as in Fig. 2.

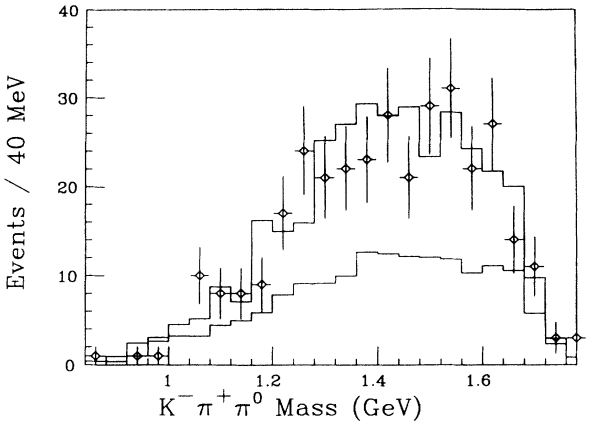

FIG. 18. $K^-\pi^+\pi^0$ invariant mass for events with the $K^-\pi^+\pi^+\pi^0$ mass in the D^+ region. The data are depicted as in Fig. 2.

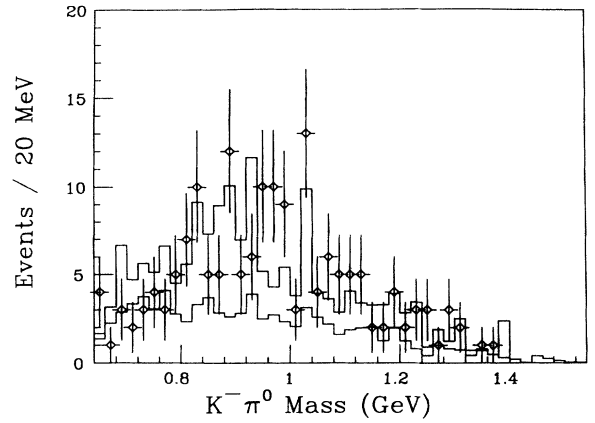

FIG. 16. $K^-\pi^0$ invariant mass for events with the $K^-\pi^+\pi^+\pi^0$ mass in the D^+ region. The data are depicted as in Fig. 2.

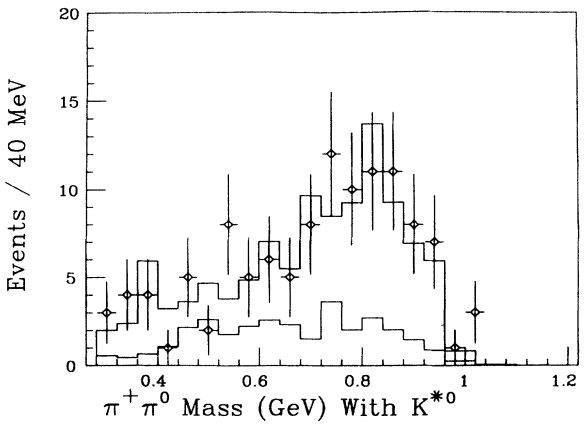

FIG. 19. $\pi^+\pi^0$ invariant mass for events with the $K^-\pi^+$ mass in the K^{*0} region. The data are from $K^-\pi^+\pi^+\pi^0$ events in the D^+ region and are depicted as in Fig. 2.

TABLE VIII. Comparison of two-body decay branching fraction results with experimental results from Mark III [7] and theoretical predictions from Wirbel, Stech, and Bauer (WSB) [3]. All branching fractions are expressed in %.

Channel	E691	Mark III	WSB
$\bar{K}^{*0}\rho^0$	1.8±0.3±0.3	1.9±0.3±0.7	6
$\bar{K}^{*0}\rho^+$	2.3±1.2±0.9	4.8±1.2±1.4	17
$K^- a_1^+(1260)$	8.6±1.2±1.9	9.0±0.9±1.7	5
$\bar{K}^0 a_1^+(1260)$	11.6±2.9±3.2	7.1±1.8±1.1	3.8
$K^- a_2^+(1320)$	≤0.2	≤0.6	
$\bar{K}^0 a_2^+(1320)$	≤0.3	≤0.8	
$K_1^-(1270)\pi^+$	≤1.3	1.8±0.5±0.8	
$\bar{K}_1^0(1270)\pi^+$	≤0.7	≤1.1	
$\bar{K}_1^0(1400)\pi^+$	≤0.9	4.1±1.2±1.2	
$(K^-\pi^+\pi^+\pi^-)_{\text{non 2 body}}$	3.5±0.6	4.2±1.7	
$(\bar{K}^0\pi^+\pi^+\pi^-)_{\text{non 2 body}}$	3.5±1.9	1.1±0.8	
$(K^-\pi^+\pi^+\pi^0)_{\text{non 2 body}}$	4.8±1.9	2.0±1.2	

terms in determining the systematic error.

The level of $K^{*-}\pi^+\pi^+$ remained a constant regardless of which angular momentum component was chosen. However, the fit was significantly better using the $K^{*-}\pi^+\pi^+$ term with no angular dependence, which indicates a mixture of angular momentum components. A $\bar{K}_1^0(1400)\pi^+$ term however, never improved the fit. This contrasts with the Mark III results [7] where they found $(27.7\pm4.7\pm8.0)\%$ of $\bar{K}_1^0(1400)\pi^+$. Systematic errors for the best fit were chosen to cover the range of fractions found from reasonable fits within 4 units in log likelihood. If the nonresonant term was left out of the fit, the log likelihood dropped by 20 units. We therefore choose to quote a fraction for it and not an upper limit, even though with the systematic error included the result is marginally significant. Figures 10–12 show the two-body projections for the best fit. Figure 13 shows the $\bar{K}^0\pi^-\pi^+$ mass spectrum for events with the $\bar{K}^0\pi^-$ mass in the K^{*-} region, and Fig. 14 shows the $\pi^+\pi^-\pi^+$ mass with the highest mass $\pi^+\pi^-$ mass combination in the ρ region.

VI. $D^+ \to K^-\pi^+\pi^+\pi^0$

For this decay the following decay channels were considered: (1) non-resonant four-body; (2) three-body $K^-\rho^+\pi^+$; (3) three-body $\bar{K}^{*0}\pi^+\pi^0$; (4) $\bar{K}_1^0(1270)\pi^+$, $K_1 \to K^-\rho^+$; (5) $\bar{K}_1^0(1400)\pi^+$, $K_1 \to K^{*-}\pi^+$, $K_1 \to \bar{K}^{*0}\pi^0$; and (6) $\bar{K}^{*0}\rho^+$ in a relative $L=0$, 1, and 2 state. As before, all combinations of the three-body decays in relative s wave and p wave were considered.

The best fit included five terms: $K^-(\rho^+\pi^+)_s$, $(\bar{K}^{*0}\pi^+)_s\pi^0$, $K^{*-}\pi^+\pi^+$ with phase space, $(\bar{K}^{*0}\rho^+)_{L=0}$, and $(\bar{K}^{*0}\rho^+)_{L=2}$. Table VI shows the subcomponent fraction, branching fraction and phase of each component. After finding that the major resonant contribution was from $\bar{K}^{*0}\pi^+\pi^0$, that phase was fixed to zero. Table VII shows the upper limits of the other terms when added into the best fit one at a time. Notice that the $\bar{K}_1^0(1270)\pi^+$ term gives a very large limit. We choose to quote the limit obtained using the higher statistics mode $D^+ \to \bar{K}^0\pi^+\pi^+\pi^-$ which is much more sensitive.

Table VI gives the branching fraction for $K^-\rho^+\pi^+$ as opposed to the specific angular component. Other angular components that gave a log likelihood within a few units of the best fit were used to determine this number. The $K^-\rho^+\pi^+_{\text{tot}}$ entry in Table VI includes all contributions that have a ρ^+ component, not just the three-body component. The total $\bar{K}^{*0}$ contribution is also given. The small errors on the these total resonance fractions show the stability over a wide choice of decay channels included in the fit. Contrary to Mark III [7], we do not observe a $\bar{K}_1^-(1400)\pi^+$ component but observe a three-body $\bar{K}^{*0}\pi^+\pi^0$ component instead. The results of the $K^-\pi^+\pi^+\pi^0$ analysis agree with those from the $D^+ \to \bar{K}^0\pi^+\pi^+\pi^-$ analysis in channels common to both decays.

Figures 15–19 show the fitted results for some two-body and three-body projections. The $K^-\pi^+$ mass plot shows a clear enhancement at the $\bar{K}^{*0}$ mass; however, the $\pi^+\pi^0$ and $K^-\pi^0$ plots show no clear resonances. It would be very hard to see a ρ^+ component of almost 50% because of its large width and because there are two combinations per event. One should expect to see the fraction $(0.20\pm0.12)\pi^+\pi^0$ events in the ρ^+ region in events opposite a $\bar{K}^{*0}$.

VII. CONCLUDING REMARKS

Table VIII compares the two-body results reported in this paper with measurements from Mark III [7] and the predictions of Wirbel, Stech, and Bauer (WSB) [3]. The most striking discrepancy with the WSB model is the much lower results in the VV channels $D^0 \to \bar{K}^{*0}\rho^0$ and $D^+ \to \bar{K}^{*0}\rho^+$. This confirms a pattern seen in other VV decays such as $D_s^+ \to \phi\rho^+$ and $D^0 \to K^{*-}\rho^+$ [7,9,10]. This may be related to the small branching fraction observed in the semileptonic decays $D^+ \to \bar{K}^{*0}e^+\nu_e$ and $D^0 \to K^{*-}e^+\nu_e$ [11–14]. As an example, in the factorization picture of WSB, the VV decay rate for $D^+ \to \bar{K}^{*0}\rho^+$ is dominated by the form factor $A_1(q^2)(q^2=m_\rho^2)$, which also controls the semileptonic rate. On the other hand, there is some question whether one expects factorization to work in the two-body modes with such low final state momentum.

The largest branching fraction seen is in the mode $\bar{K}^0 a_1^+(1260)$, which is also larger than the WSB prediction. Indeed this is one of the largest branching fractions yet measured. The $D^0 \to K^- a_1^+(1260)$ branching fraction is also larger than the WSB prediction. Both of these are also larger than the prediction of Kamal [4]. Kamal also suggests that final-state interactions will not enhance the branching fraction predictions. The measurements are generally in agreement with the Mark III [7] results except in the mode $\bar{K}_1^0(1400)\pi^+$ where we see no signal.

ACKNOWLEDGMENTS

We gratefully acknowledge the assistance of the staff of Fermilab and of all the participating institutions. This research was supported by the U.S. Department of Energy, by the U.S. National Science Foundation, by the Natural Sciences and Engineering Research Council of Canada through the Institute for Particle Physics, by the National Research Council of Canada, and by the Brasilian Conselho Nacional de Desenvolvimento Científico e Technológico.

[1] L. L. Chau and H. Y. Cheng, Phys. Rev. D **36**, 137 (1987).
[2] B. Y. Blok and M. A. Shifman, Sov. J. Phys. **45**, 522 (1987).
[3] M. Wirbel, B. Stech, and M. Bauer, Z. Phys. C **34**, 103 (1987).
[4] A. N. Kamal, R. C. Verma, and N. Sinha, Phys. Rev. D **43**, 843 (1991); A. N. Kamal and R. C. Verma, *ibid.* **45**, 982 (1992).
[5] Particle Data Group, J. J. Hernández *et al.*, Phys. Lett. B **239**, 1 (1990).
[6] J. Adler *et al.*, Phys. Rev. Lett. **60**, 89 (1988).
[7] D. F. DeJongh, Ph.D. thesis, California Institute of Technology, 1990; D. Coffman *et al.*, Phys. Rev. D **45**, 2196 (1992).
[8] J. R. Raab *et al.*, Phys. Rev. D **37**, 2391 (1988).
[9] J. C. Anjos *et al.*, Phys. Rev. B **223**, 267 (1989).
[10] CLEO Collaboration, M. Daoudi *et al.*, Phys. Rev. D **45**, 3965 (1992).
[11] J. C. Anjos *et al.*, Phys. Rev. Lett. **62**, 1587 (1989).
[12] Z. Bai *et al.*, Phys. Rev. Lett. **66**, 1011 (1991).
[13] J. Alexander *et al.*, Phys. Rev. Lett. **65**, 1531 (1990).
[14] H. Albrecht *et al.*, Phys. Lett. B **255**, 634 (1991).